Modulation by Ca^{2+} and by Membrane Binding of the Dynamics of Domain III of Annexin 2 (p36) and the Annexin 2−p11 Complex (p90): Implications for Their Biochemical Properties†

Jesus Ayala-Sanmartin,‡ Michel Vincent,§ Jana Sopkova,|| and Jacques Gallay*,§

Unité de Biologie Cellulaire et Moléculaire de la Sécrétion, Institut de Biologie Physico-Chimique, 13 rue Pierre et Marie Curie, F-75005 Paris, France, UFR des Sciences Pharmaceutiques, 5 rue Vaubenard, F-14032 Caen, France, and LURE Laboratoire pour l'Utilisation du Rayonnement Electromagnétique, Université Paris-Sud, Bâtiment 209D, BP 34, F-91898 Orsay Cedex, France

Received March 3, 2000; Revised Manuscript Received September 20, 2000

ABSTRACT: The modulation of the local structure and dynamics of domain III of annexin 2 (Anx2), in both the monomeric (p36) and heterotetrameric forms (p90), by calcium and by membrane binding was studied by time-resolved fluorescence intensity and anisotropy measurements of the single tryptophan residue (W212). The results yield the same dominant excited-state lifetime (1.4 ns) in both p36 and p90, suggesting that the conformation and environment of W212 are very similar. The fluorescence anisotropy decay data were analyzed by associative (two-dimensional) as well as nonassociative (one-dimensional) models. Although no statistical criterion is decisive for one model versus the other, only the associative model allows recovery of a physically relevant value of the Brownian rotational correlation of the protein. Using the associative model, a nanosecond flexibility is detectable in p90 but not in p36. When Ca^{2+} binds in the millimolar concentration range to both forms of Anx2, a conformational change takes place leading to an increase of the major excited-state lifetime (2.6 ns) and to a suppression of the W212 local flexibility of p90. Binding to membranes of either p36 or p90 in the presence of Ca^{2+} does not induce any conformational change other than that provoked by Ca^{2+} binding alone. The W212 local flexibility in both proteins increases significantly, however, in their membrane-bound forms. In the presence of membranes, the conformation change of domain III in p90 displays a sensitivity to Ca^{2+} 2 orders of magnitude higher than that of p36, reaching intracellular sub-micromolar concentration ranges. This higher Ca^{2+} sensitivity correlates with the Ca^{2+}-dependent membrane aggregation but not with their Ca^{2+}-dependent binding to membranes. The significance of these structural and dynamical changes for the function of the protein is discussed.

Annexins constitute a family of water-soluble proteins, which undergo reversible Ca^{2+}-dependent binding to phospholipid bilayers and specific cellular membranes (*1*−*3*). Anx2[1] is a major cytoplasmic substrate of the $pp60^{src}$ tyrosine kinase (*4*−*6*). This protein is found either as a monomer (p36) or as a heterotetramer (p90) when two Anx2 molecules are associated with a dimer of p11, an S100-like protein devoid of tryptophan residues (*7*, *8*). It is likely involved in cellular events such as exo- and endocytosis (*9*−*14*). Like the other members of the annexin family, it consists of two parts: the highly variable N-terminal segment and the conserved "core". The N-terminal sequence of Anx2 contains 30 residues and has been shown to regulate the membrane binding and aggregation capacities of the core (*15*, *16*) (J. Ayala-Sanmartin, unpublished results). The N-terminal tail encompasses the site for p11 binding (1−14 residues) (*17*−*20*) and the regions for phosphorylation by $pp60^{src}$ tyrosine kinase (Tyr23) and by protein kinase C (residues 11−25) (*21*−*24*). The core consists of four repeats, each about 70 residues in length as in the majority of annexins. It shares important sequence and structural homologies with the other members of the family. The crystal structure of Anx2 shows that these repeats correspond to structural domains consisting of five α-helices (A−E) (*25*). Two classes of Ca^{2+} binding sites have been characterized in Anx2: high-affinity type II and low-affinity type III sites (*26*, *27*). Only one type III Ca^{2+} binding site is present in domain I with a low affinity ($K_d \sim 200\ \mu M$). The other domains contain one high-affinity type II Ca^{2+} binding site ($K_d \sim 10\ \mu M$). The crystal structure (*25*) and mutagenesis experiments (*26*, *28*) have shown that the type II sites are defined by the sequence $GXGT(X)_{38}D$ for domains II and IV and $RKGT(X)_{38}E$ for domain III. However, the calcium binding capacity of the protein in the

† This work was supported by the Centre National de la Recherche Scientifique (UPR 1929 and UMR 130). M.V. acknowledges the Institut National de la Santé et de la Recherche Médicale for continuous support.

* To whom correspondence should be addressed: LURE, Université Paris-Sud, Bâtiment 209D, BP 34, F-91898 Orsay Cedex, France. Fax: 33 1 64 46 80 82. E-mail: gallay@lure.u-psud.fr.

‡ Institut de Biologie Physico-Chimique.

§ Université Paris-Sud.

|| UFR des Sciences Pharmaceutiques.

[1] Abbreviations: Anx2, annexin 2; Anx3, annexin 3; Anx5, annexin 5; PC, L-α-phosphatidylcholine; PS, L-α-phosphatidylserine; p36, Anx2 monomer; p90, $(Anx2)_2-(p11)_2$ heterotetramer; MEM, maximum entropy method; SUVs, small unilamellar vesicles.

10.1021/bi000501x CCC: $19.00
Published on Web 11/16/2000

presence of lipids is higher than expected on the basis of crystallographic data. The p36 monomer and the p90 can bind 10−11 and 12−15 Ca^{2+} ions, respectively (*29*).

Anx2 possesses a single tryptophan residue (W212) in domain III, buried inside the protein and located in the middle of α-helix IIIB, which allows detailed fluorescence studies of this region (*26*, *28*, *30*−*32*). An H-bond interaction is formed between the N_ϵ atom of the indole ring and the carbonyl group of L197 in α-helix IIIA (*25*). The conformation of Anx2 without Ca^{2+} ion in domain III is still unknown. However, steady-state and time-resolved fluorescence studies have shown that calcium binding induces a conformational change in domain III (*26*, *28*, *30*−*32*). The RKGT loop of the calcium-binding site in domain III becomes more resistant to trypsin cleavage at R204 and K205 (*26*). The absorbance of p90 between 270 and 290 nm is decreased in the presence of Ca^{2+} (*7*). In the presence of negatively charged phospholipid membranes, the apparent affinity of the protein for calcium is increased (*1*, *15*, *16*, *29*). This effect is more pronounced for the heterotetramer than for the monomer (*16*). The structural basis of this phenomenon remains obscure. Additional conformational changes induced by Ca^{2+}-dependent binding at the membrane surface have been proposed to explain this increased calcium sensitivity (*31*). An alternative possibility could be that the assembly of a protein with eight repeating units such as p90 to phospholipidic membranes could reduce the calcium requirement for its binding with respect to p36, which contains only four principal Ca^{2+} binding sites (*29*, *33*, *34*).

To gain more accurate insight into the local conformational and dynamical changes provoked by calcium and membrane binding of p36 and of p90, a detailed time-resolved fluorescence intensity and anisotropy study of the single tryptophan residue W212 was initiated. We show that Ca^{2+} binding modifies the local conformation of W212 but that no further change is brought about upon binding to the membrane surface for neither p36 nor p90. The local dynamics sensed by W212 is, however, significantly enhanced at the membrane surface for both proteins, but more for p90 than for p36. In addition, the observed conformational change correlates with the aggregation capacity of the proteins. We propose a model in which Ca^{2+} binding triggers the observed conformational change of domain III at the membrane surface. The reduction in the calcium level required for aggregation of membranes could be related to Ca^{2+}-induced cooperativity effects instead of a membrane-induced conformational change.

MATERIALS AND METHODS

Materials. Bovine brain type III-B PC and PS were obtained from Sigma. All other chemicals were analytical grade.

Protein Preparation. The human Anx2 heavy chain cDNA generously provided by E. Solito and F. Russo-Marie (ICGM, Hôpital Cochin, Paris, France) was subcloned in the *Saccharomyces cerevisiae* vector pYeDP60 kindly provided by D. Pompon (CNRS, Gif-sur-Yvette, France) by a strategy to be published elsewhere (J. Ayala-Sanmartin et al., manuscript submitted for publication). A pET-23a vector containing the human p11 cDNA (kind gift of V. Gerke, Munster, Germany) was used for expression of p11 in *Escherichia coli* cells. Both recombinant human proteins were expressed and purified by procedures described elsewhere (J. Ayala-Sanmartin et al., manuscript submitted for publication). The degree of purity (>98%) and the biochemical characterization (immunoreactivity, p36−p11 association) of the proteins will be published elsewhere (J. Ayala-Sanmartin et al., manuscript submitted for publication). The Edman degradation assay of p36 indicated that the N-terminal extremity is blocked, suggesting the acetylation of the first serine in the yeast-produced protein as has been reported for annexin 1 (*35*). The heterotetramer (p90) was obtained by incubation of the p36 and p11 chains at a molar ratio of 1:1. The properties of the reconstituted recombinant p90 were identical to those of the lung tetramer in the chromaffin granule aggregation assay (not shown).

Phospholipid Vesicle Preparation. PC/PS (75/25) SUVs were obtained by extrusion of large multilamellar vesicles as previously described (*36*) in a calcium-buffered solution containing 40 mM HEPES (pH 7), 30 mM KCl, and 1 mM EGTA at a final lipid concentration of 2.5 mg/mL. Before the fluorescence experiments, the SUV suspension was sonicated for 5 min on ice.

Binding of the Proteins to Membrane Vesicles and Aggregation of Liposomes. Anx2 binding to membranes and SUV aggregation were performed in the same buffer as described above. The free Ca^{2+} concentrations (pCa = colog-$[Ca^{2+}]_{free}$) were calculated with the Calcv22 program (*37*). The level of protein binding was measured by copelleting the proteins with the liposomes after centrifugation at 170000*g* for 30 min. The pellets were solubilized in SDS, and the amount of Anx2 was quantified (*36*). Liposome aggregation was monitored by measuring the increase in turbidity at 340 nm and 28 °C (*36*).

Preparation of the Protein Samples for Fluorescence Measurements. The fluorescence measurements were performed at 20 °C in 100 μL microcuvettes with an optical path of 10 mm × 2 mm (Hellma, France). The free calcium concentration was obtained by adding the $CaCl_2$ quantities calculated as described above (*37*). The protein concentration values, obtained with the Coomassie assay reagent (Pierce) using BSA as a standard, were corrected on the basis of the specific absorbance at 280 nm (*7*). The final protein concentrations in the assays were 10 μM for the p36 monomer and 5 μM for the p90 heterotetramer (10 μM total p36). When sonicated SUVs were present, the total phospholipid concentration was 1 mM (125 μM accessible PS).

Time-Resolved Fluorescence Measurements. Fluorescence intensity and anisotropy decays were obtained by the time-correlated single-photon counting technique from the polarized components $I_{vv}(t)$ and $I_{vh}(t)$ on the experimental setup installed on the SB1 window of the synchrotron radiation machine Super-ACO (Anneau de Collision d'Orsay) (*38*). The excitation wavelength was selected with a double-grating monochromator (Jobin Yvon UV-DH10, bandwidth of 4 nm), and the emission wavelength was selected with a single-grating monochromator (Jobin Yvon UV-H10, bandwidth of 8 nm). Detection was performed with a MCP-PMT Hamamatsu apparatus (model R3809U-02). The time resolution was ∼20 ps. The histograms were stored in 2048 channels. Automatic sampling cycles, including an accumulation time of 30 s for the instrument response function and an acquisition time of 90 s for each polarized component, were

carried out so that a total number of $2-4 \times 10^6$ counts was reached in the fluorescence intensity decay.

Data Analysis of Fluorescence Intensity and Anisotropy Decays. Analyses of fluorescence intensity decays as sums of exponential terms were performed by the maximum entropy method (MEM) (*39*−*41*). Analyses of the polarized fluorescence decays were performed by two programs. The first one is based on a one-dimensional model of the anisotropy, in which each lifetime τ_i is coupled to every rotational correlation time θ_i (*41*, *42*). The second program is based on a two-dimensional (τ and θ) model, which allows us to describe the coupling between lifetimes and rotational correlation times (*41*, *43*−*45*). This latter model starts without any a priori (τ and θ) coupling, the MEM program being able to handle a considerable number of independent variables. There is nevertheless an inherent limit to the method since the parallel and perpendicular components of the polarized decay involve in their expressions a harmonic mean κ_i between τ_i and θ_i: $1/\kappa_i = 1/\tau_i + 1/\theta_i$, where τ_i and θ_i can be exchanged without any modification in the κ_i value, leading to construction of iso-κ curves. These iso-κ contours are visualized on the two-dimensional (τ and θ) maps by dotted lines. This degeneracy is especially troublesome when short lifetimes are coupled to long correlation times and conversely as shown by simulations (*41*). Calculations with double precision allows minimization of this problem to a large degree.

Fluorescence intensity and one-dimensional anisotropy decay analyses were performed on a DEC Vax station 4000/90 computer. Sets of 150 and 100 independent variables, equally spaced in log scale, were used for the fluorescence intensity and anisotropy decays, respectively. The two-dimensional analyses were carried out on a DEC alpha Vax 7620 computer. A set of 1600 independent variables (40 τ values and 40 θ values) was used for this analysis. The programs including the MEMSYS 5 subroutines (MEDC Ltd., Cambridge, U.K.) were written in double-precision FORTRAN 77.

RESULTS

Effect of Calcium Binding to p36 and p90 on the Excited-State Lifetime Distribution: Local Conformation and Dynamics around W212. In the absence of calcium, the fluorescence emission spectrum of the W212 residue in p36 exhibits a maximum at around 320 nm (*26*, *28*, *30*, *31*). The fluorescence decay of W212 at the maximum of emission is not monoexponential (Figure 1). A major excited-state lifetime population centered at 1.4 ns characterizes it, which represents 70−80% of the distribution (Figure 2A and Table 1). Two minor peaks corresponding to shorter and longer lifetimes are also detected. The same pattern is observed at the emission wavelength of 340 nm (not shown). Binding of calcium ion induces a blue shift in the fluorescence emission spectrum (from 320 to ∼312 nm) (*26*, *28*, *30*, *31*), which is accompanied by a significant change in the intensity decay (Figure 1B). In the presence of Ca^{2+}, the excited-state lifetime distribution is characterized by a major component of 2.6 ns, longer than in the absence of the ion (Figure 2B and Table 1). It becomes largely dominant at calcium concentrations in the millimolar range (Figure 3A, where only the data for the 2.6 ns component are presented). The midrange effect of Ca^{2+} takes place at ∼0.7 mM.

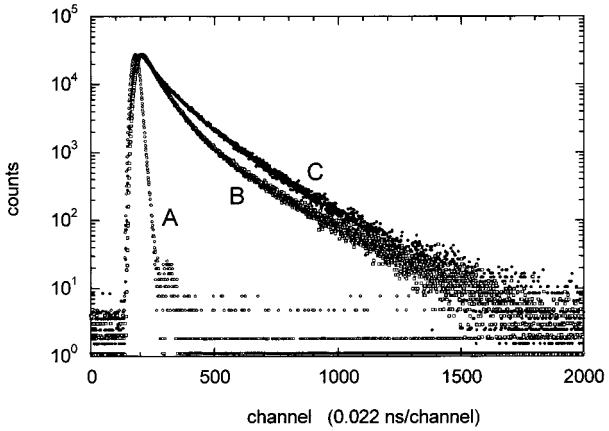

FIGURE 1: Experimental fluorescence intensity decays of W212 in p36. The excitation wavelength was 295 nm and the emission wavelength 325 nm. (A) Instrumental response function. (B) p36 without Ca^{2+}. (C) p36 in the presence of free 3 mM Ca^{2+} (pCa = 2.5).

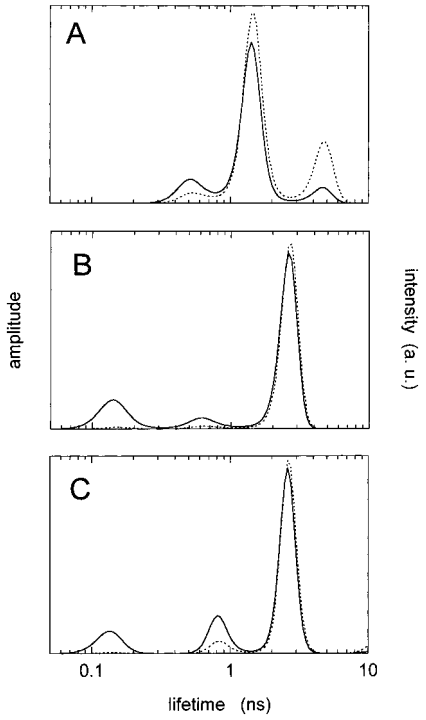

FIGURE 2: Excited-state lifetime distributions (—) and intensity-weighted contribution (···) recovered by MEM of W212 in the Anx2 monomer (p36). MEM analysis as a sum of exponentials was performed on the fluorescence intensity $T(t)$ reconstructed from the parallel and perpendicular polarized components $I_{vv}(t)$ and $I_{vh}(t)$ as explained in the footnote of Table 1: (A) calcium-free buffer, (B) 2 mM free Ca^{2+} (pCa = 2.7), and (C) 1 mM free Ca^{2+} (pCa = 3) in the presence of sonicated SUVs (lipid/protein molar ratio of 100). The excitation wavelength was 295 nm and the emission wavelength 320 nm. The protein concentration was 10 μM.

Similar observations are obtained for the p90 complex. Binding of p11 does not lead to any significant change in the excited-state lifetime distribution of W212 (Figure 4A). Ca^{2+} depresses the 1.4 ns lifetime proportion to the benefit of the 2.6 ns lifetime population as in p36 (Figure 4B and Table 1). Minor peaks with shorter and longer lifetime center values are also present. The midrange effect of ion binding on the respective lifetime amplitude values occurs in the same range of calcium concentrations for both p90 and p36 (0.7 mM) (Figure 3).

Table 1: Effect of Ca^{2+} and SUVs on the Fluorescence Intensity Decay Parameters Recovered by MEM of the W212 Emission in Monomeric p36 and Heterotetrameric p90[a]

sample	τ_1 (ns),[b] C_1,[c] I_1[d]	τ_2 (ns), C_2, I_2	τ_3 (ns), C_3, I_3	$\langle t \rangle$ (ns)[e]
p36	0.55 ± 0.03, 0.20 ± 0.03, 0.08	1.41 ± 0.01, 0.71 ± 0.06, 0.69	4.23 ± 0.29, 0.08 ± 0.01, 0.23	1.45
p36 (pCa = 3)[f]	0.17 ± 0.06, 0.15 ± 0.04, 0.01	0.74 ± 0.44, 0.12 ± 0.07, 0.04	2.58 ± 0.12, 0.73 ± 0.09, 0.95	1.99
p36 (pCa = 3)[f] (L/P = 100)	0.26 ± 0.17, 0.13 ± 0.01, 0.02	1.08 ± 0.34, 0.18 ± 0.01, 0.10	2.59 ± 0.01, 0.69 ± 0.01, 0.88	2.03
p90	0.51 ± 0.03, 0.22 ± 0.02, 0.08	1.47 ± 0.01, 0.71 ± 0.03, 0.70	4.76 ± 0.16, 0.07 ± 0.01, 0.22	1.49
p90 (pCa = 3)[f]	−	0.60 ± 0.05, 0.17 ± 0.02, 0.05	2.56 ± 0.01, 0.82 ± 0.03, 0.95	2.20
p90 (pCa = 4.7)[f] (L/P = 100)	−	0.51 ± 0.05, 0.25 ± 0.02, 0.07	2.39 ± 0.02, 0.75 ± 0.03, 0.93	2.14

[a] MEM analysis was performed on the fluorescence intensity $T(t)$ reconstructed from the parallel and perpendicular polarized components $I_{vv}(t)$ and $I_{vh}(t)$ such as $T(t) = I_{vv}(t) + 2\beta_{corr}I_{vh}(t) = \int_0^\infty \alpha(\tau) \exp(-t/\tau)\, d\tau$, where τ is the excited-state lifetime, $\alpha(\tau)$ is its amplitude, β_{corr} is a correction factor accounting for the difference in transmission of the $I_{vv}(t)$ and $I_{vh}(t)$ components (*66*). Standard deviations for three measurements are reported. [b] τ_i values are the centers of each lifetime peak. [c] C_i values are the normalized amplitudes of each lifetime peak. [d] I_i values are the values of the partial intensity of the ith component $I_i = C_i\tau_i$. [e] The mean lifetime $\langle \tau \rangle$ is calculated as $\langle \tau \rangle = \Sigma_i \alpha_i \tau_i$. [f] Defined in Materials and Methods.

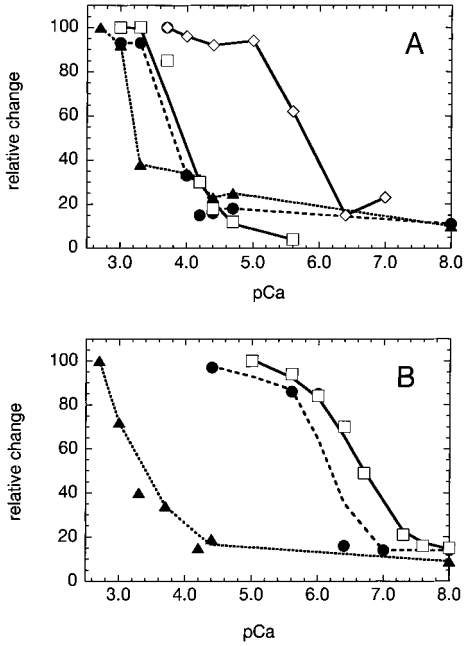

FIGURE 3: Ca^{2+} dependence of conformational change, membrane binding, and membrane aggregation properties of p36 and p90. Amplitude of the major excited-state lifetime of 2.6 ns (C_3 in Table 1): (▲) in the absence of SUV, (●) in the presence of SUV (lipid/protein molar ratio of 100), (◇) membrane binding, and (□) membrane aggregation. (A) p36 and (B) p90. Results are represented as percentages of the maximal response.

Mobility of W212 in p36 and p90: Effect of Ca^{2+}. The experimental fluorescence anisotropy decay of p36 in the absence of calcium indicates a fast depolarization process in the time region where the instrument response function affects the profile, followed by a much slower one (Figure 5A). To cast off the distortion of the decay curve by the

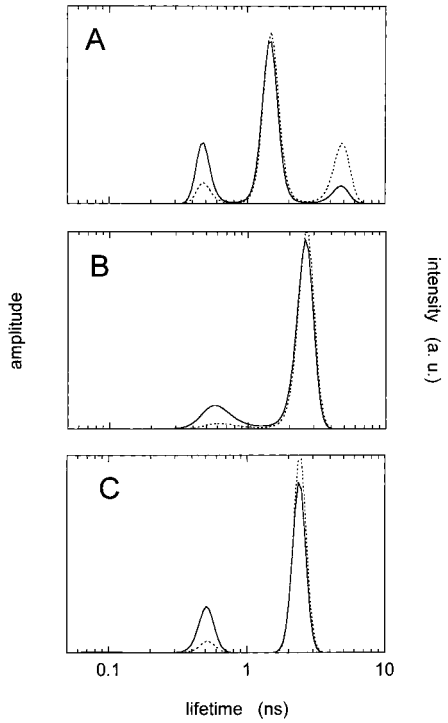

FIGURE 4: Excited-state lifetime distributions (—) and intensity-weighted contribution (···) of W212 obtained by MEM of the Anx2 tetramer (p90) in (A) Ca^{2+}-free buffer, (B) 1 mM free Ca^{2+} (pCa = 3), and (C) 20 μM free Ca^{2+} (pCa = 4.7) in the presence of sonicated SUVs (lipid/protein molar ratio of 100). The excitation wavelength was 295 nm and the emission wavelength 320 nm. The protein concentration was 5 μM (10 μM p36).

instrument response function, the impulse fluorescence anisotropy decay $A_{imp}(t)$ was calculated as $[I_{imp,vv}(t) - I_{imp,vh}(t)]/[I_{imp,vv}(t) + 2I_{imp,vh}(t)]$, where $I_{imp,vv}(t)$ and $I_{imp,vh}(t)$ are the impulse decays for the vertical and horizontal components obtained after separate deconvolution, respectively (Figure 5B). The impulse anisotropy decay does not likely follow a simple multiexponential law. Indeed, the derivative of the curve increases at short times and then exhibits a maximum near 1 ns, whereafter it decreases (not shown). Such a pattern is typical of a system in which short lifetimes are coupled to fast rotations and long lifetimes to slow ones (*46*, *47*), as previously shown for different chromophores such as ethidium bromide (*41*), parinaric acids (*48*, *49*), tryptophan (*43*), dansyl (*50*), and anthraniloyl nucleotide derivatives (unpublished results). An analytical representation of the impulse anisotropy decay like that shown in Figure 5B using a sum of exponentials (classical model) is not relevant if the signs of the amplitudes are strictly positive, a situation corresponding to the particular case where each emitting population is coupled to every rotational motion. The best fit is only obtained when negative amplitudes (without physical meaning) are allowed (Figure 5B).

To analyze these types of data, methods mainly based on nonlinear least-squares regression have been developed in the literature but involving imposed $\tau-\theta$ associations (*46*, *48*−*51*). On the contrary, MEM allows a non-a priori guess with respect to the $\tau-\theta$ associations using the two-dimensional analysis of the fluorescence-polarized decays (*43*−*45*, *52*). It exhibits moreover the advantage of exploring a wide $\tau-\theta$ space. Both models (one- and two-dimensional) will be discussed in this work along with their ability to analyze the data.

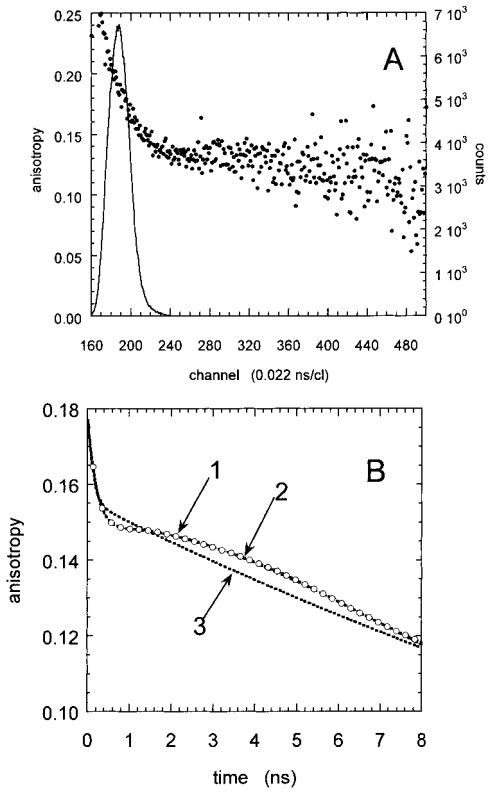

FIGURE 5: (A) Experimental anisotropy decay curves $A(t)$ of p36 calculated from the experimental polarized fluorescence decays $I_{vv}(t)$ and $I_{vh}(t)$ (see the footnote of Table 2). (B) Impulse anisotropy decay curves calculated after deconvolution of $I_{vv}(t)$ and $I_{vh}(t)$ (curve 1 with empty points), the best fit with a quadruple exponential without assumption of the amplitude signs (dotted curve 2), and the best fit with a quadruple exponential with only positive pre-exponents (dotted curve 3).

Table 2: Effect of Calcium Binding on the Fluorescence Anisotropy Decay Parameters Recovered after MEM Analysis Using the One-Dimensional Model of W212 in p36 and p90[a]

sample	θ (ns)[b]	β[c]	ω_{max} (deg)[d]
p36	34 ± 2	0.151 ± 0.012	33 ± 4
p36 (pCa = 2.7)	28 ± 1	0.185 ± 0.011	25 ± 4
p90	45 ± 2	0.148 ± 0.011	33 ± 4
p90 (pCa = 3)	44 ± 3	0.178 ± 0.013	27 ± 5

[a] The fluorescence anisotropy is assumed to be described by a sum of exponentials: $A(t) = I_{vv}(t) - \beta_{corr} I_{vh}(t)/I_{vv}(t) + 2\beta_{corr} I_{vh}(t) = \Sigma_i \beta_i \exp(-t/\theta_i)$. β_{corr} is the correction factor defined in the legend of Table 1. [b] Values of the barycenter of the rotational correlation time peaks. [c] Partial anisotropy. [d] The wobbling-in-cone angle ω_{max} value was calculated according to $\beta/A_0 = [1/2 \cos \omega_{max}(1 + \cos \omega_{max})]^2$ (*54*). A value of the intrinsic anisotropy A_0 of 0.25 was used. The excitation wavelength was 295 nm.

Despite the shape of the impulse fluorescence decay of W212 (Figure 5B), the analysis by the one-dimensional model of anisotropy provides reasonably low χ^2 values ($\sim$1). Only one long rotational correlation time, describing in principle the Brownian rotation of the entire protein, is observed (Table 2). Rotational motions faster than the detection limit of the instrumentation are probably taking place since the initial anisotropy is lower than expected for an immobilized tryptophan residue (*53*). A semiangle of the wobbling-in-cone motion (ω_{max}) can be calculated (*54*) (Table 2). The value of the Brownian rotational correlation time is, however, larger than expected for a spherical particle of the size of the protein with 40% (w/w) hydration, according to the Perrin−Einstein expression ($\theta = V_h \eta/RT$, where V_h is the hydrated volume of the particle, η the solvent viscosity, R the molar gas constant, and T the absolute temperature). Anx5, for instance, which displays the same shape of the core and a similar molecular weight, exhibits the expected Brownian rotational correlation time value of 14.5−15 ns, in good agreement with its size (*44*, *55*). This model-dependent difference between the physical and the recovered values of the Brownian rotational correlation time has been observed by simulation calculations in which specific couplings between lifetimes and correlation times were modeled (M. Vincent et al., unpublished results). These anomalously larger values probably occur because the one-dimensional model cannot properly describe the anisotropy decay curve when the β values are all positive. The best fit that can be achieved with these constraints is to make the calculated curve very flat at long times, by making the Brownian rotational correlation time very large, without physical meaning (*50*). Conversely, the two-dimensional analysis allowed us to recover all the parameters of the simulation (M. Vincent et al., unpublished results).

In agreement with the observations on simulated data, the two-dimensional analysis of the p36 data is also able to recover a Brownian rotational correlation time value of $\sim$15 ns similar to that of Anx5 (*44*, *45*, *55*) (Figure 6A) and, therefore, physically significant. It also detects a fast rotational motion ($\sim$300 ps). This fast motion is strongly coupled to the shortest lifetime, which is not at all coupled to the Brownian rotational motion of the protein (Figure 6A). It seems therefore that this minor short lifetime (<10% fluorescence intensity, Table 1) corresponds to a mobile conformer, which does not detect any rotational constraint of the protein matrix. The major lifetime of 1.4 ns, on the contrary, is coupled both to this fast motion and to the Brownian rotational correlation time of the protein (Figure 6A). From the respective amplitudes $\Gamma(\tau,\theta)$ of the cross-correlation peaks in this lifetime population of 1.4 ns, a value of the semiangle of the wobbling-in-cone motion (ω_{max}) of 28° can be calculated from $\Gamma(\tau_2,\theta_3)/\Gamma(\tau_2,\theta_2) + \Gamma(\tau_2,\theta_3) = 1/2[\cos \omega_{max}(+ \cos \omega_{max})]^2$ (*54*). The $\Gamma(\tau,\theta)$ values are listed in the legend of the Figure 6.

This two-dimensional analysis provides, however, χ^2 values not significantly different from those obtained with the one-dimensional model. This statistical parameter, as well as other classical ones taking into account the number of free parameters like the F test or reduced χ^2, cannot be used as a criterion for choosing either alternate model in this particular set of data. Both solutions are apparently in the "feasible set" (*39*). However, the difference observed between the two Brownian rotational correlation time values obtained with each model is unambiguous and more in favor of the two-dimensional model.

The binding of Ca^{2+} to p36 affects the anisotropy decay parameters obtained by the one-dimensional model. It enhances the β value, which leads to a decreased value of ω_{max}, i.e., a more restrained W212 mobility (Table 2). The Brownian rotational correlation time value remains approximately the same as in the absence of Ca^{2+}. The two-dimensional analysis shows that the shortest lifetime is coupled only to the fast rotational motion, which displays a rotational correlation time similar to that in the absence of the divalent ion (Figure 6B). Therefore, as in the Ca^{2+}-free

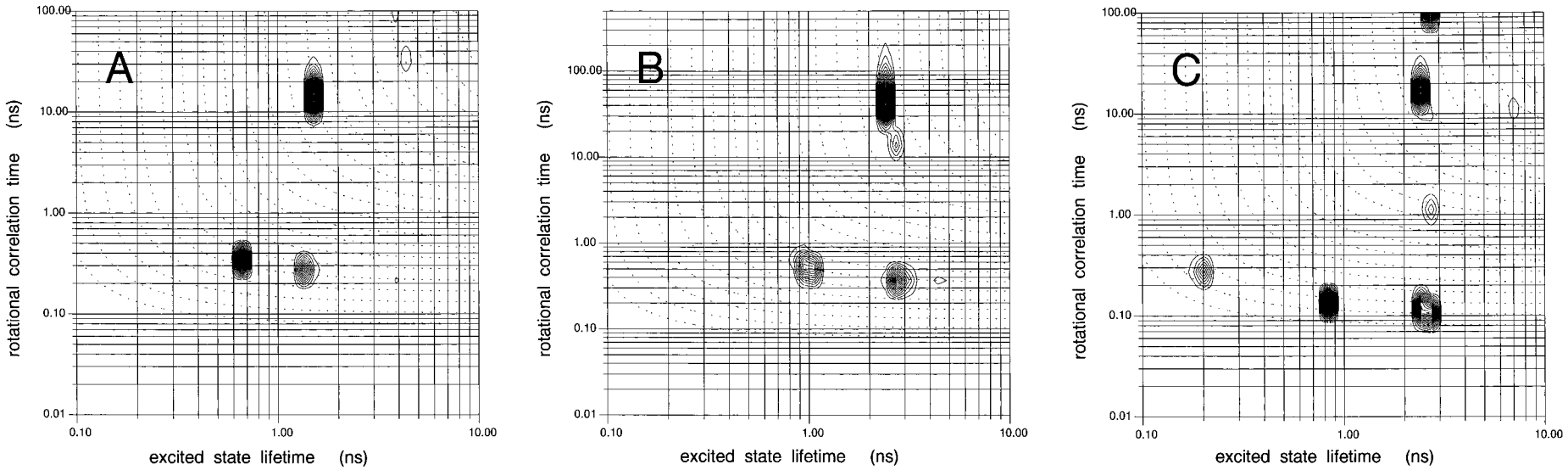

FIGURE 6: Two-dimensional plot of $\Gamma(\tau,\theta)$ coefficients obtained by MEM analysis of the polarized fluorescence decays of W212 in monomeric annexin 2. The fit was performed on the polarized fluorescence intensity decays $I_{vv}(t)$ and $I_{vh}(t)$ using the classical expressions $I_{vv}(t) = {}^1/_3\int_0^\infty\int_0^\infty\Gamma(\tau,\theta)e^{-t/\tau}(1 + 2A_0e^{-t/\theta})\,d\tau\,d\theta$ and $I_{vh}(t) = {}^1/_3\int_0^\infty\int_0^\infty\Gamma(\tau,\theta)e^{-t/\tau}(1 - A_0e^{-t/\theta})\,d\tau\,d\theta$. $\Gamma(\tau,\theta)$ is the relative proportion of emittor with a lifetime τ and a correlation time θ and A_0 is the intrinsic anisotropy taken as 0.25. (A) Ca^{2+}-free buffer. Amplitude of the (τ,θ) peak corresponding to $\tau_1 = 0.66$ ns: $\Gamma(\tau_1,\theta_1{=}0.35\text{ ns}) = 0.30$; amplitudes of the (τ,θ) peaks corresponding to $\tau_2 = 1.47$ ns: $\Gamma(\tau_2,\theta_2{=}0.28\text{ ns}) = 0.19$, $\Gamma(\tau_2,\theta_3{=}15\text{ ns}) = 0.47$; amplitudes of the (τ,θ) peaks corresponding to $\tau_3 = 4.15$ ns: $\Gamma(\tau_3,\theta_4{=}0.22\text{ ns}) = 0.02$, $\Gamma(\tau_3,\theta_5{=}30\text{ ns}) = 0.03$. (B) Free Ca^{2+} at 1 mM (pCa = 3). Amplitude of the (τ,θ) peak corresponding to $\tau_1 = 0.99$ ns: $\Gamma(\tau_1,\theta_1{=}0.50\text{ ns}) = 0.24$; amplitudes of the (τ,θ) peaks corresponding to $\tau_2 = 2.57$ ns: $\Gamma(\tau_2,\theta_2{=}0.40\text{ ns}) = 0.20$; $\Gamma(\tau_2,\theta_3{=}45\text{ ns}) = 0.51$. (C) Free Ca^{2+} at 0.5 mM (pCa = 3.3) and sonicated SUVs. Amplitude of the (τ,θ) peak corresponding to $\tau_1 = 0.20$ ns: $\Gamma(\tau_1,\theta_1{=}0.30\text{ ns}) = 0.09$; amplitude of the (τ,θ) peak corresponding to $\tau_2 = 0.84$ ns: $\Gamma(\tau_2,\theta_2{=}0.15\text{ ns}) = 0.18$; amplitudes of the (τ,θ) peaks corresponding to $\tau_3 = 2.64$ ns: $\Gamma(\tau_3,\theta_3{=}0.15\text{ ns}) = 0.28$; $\Gamma(\tau_3,\theta_4{=}1.5\text{ ns}) = 0.04$; $\Gamma(\tau_3,\theta_5{=}15\text{ ns}) = 0.26$; $\Gamma(\tau_3,\infty) = 0.15$. Measurement conditions were as described in the legend of Figure 2.

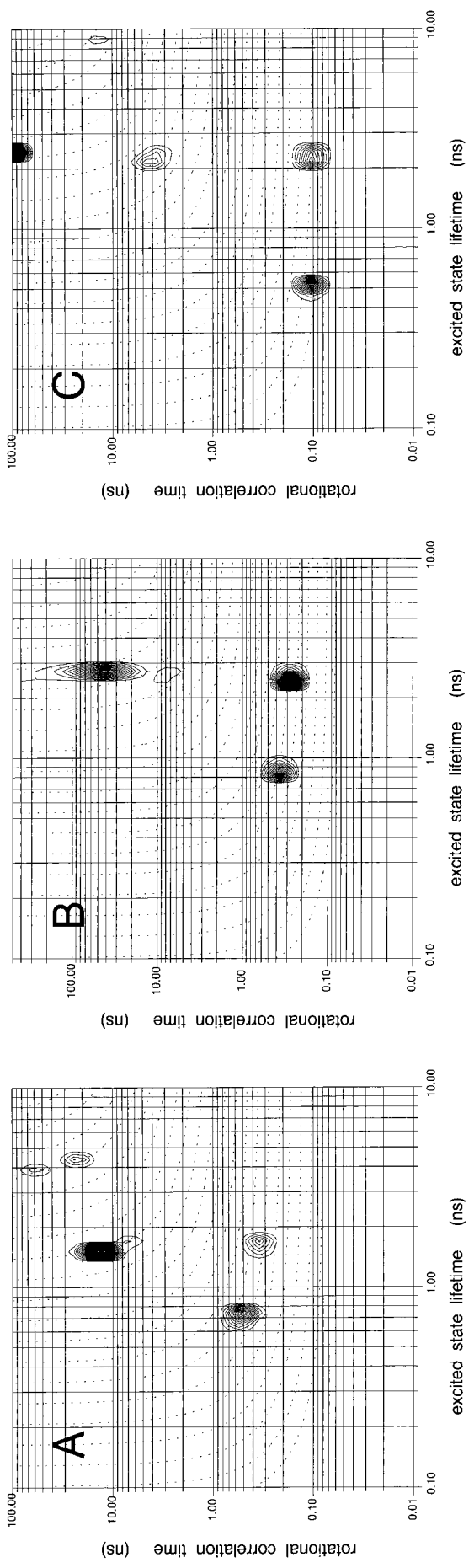

FIGURE 7: Two-dimensional plot of $\Gamma(\tau,\theta)$ coefficients obtained by MEM analysis of the polarized fluorescence decays of W212 in the tetrameric p90. (A) Ca^{2+}-free buffer. Amplitude of the (τ,θ) peak corresponding to $\tau_1 = 0.72$ ns: $\Gamma(\tau_1,\theta_1{=}0.60\text{ ns}) = 0.34$; amplitudes of the (τ,θ) peaks corresponding to $\tau_2 = 1.55$ ns: $\Gamma(\tau_2,\theta_2{=}0.35\text{ ns}) = 0.14$; $\Gamma(\tau_2,\theta_3{=}15\text{ ns}) = 0.52$. (B) Free Ca^{2+} at 1 mM (pCa = 3). Amplitude of the (τ,θ) peak corresponding to $\tau_1 = 0.87$ ns: $\Gamma(\tau_1,\theta_1{=}0.40\text{ ns}) = 0.21$; amplitudes of the (τ,θ) peaks corresponding to $\tau_2 = 2.61$ ns: $\Gamma(\tau_2,\theta_2{=}0.30\text{ ns}) = 0.30$; $\Gamma(\tau_2,\theta_3{=}8\text{ ns}) = 0.04$; $\Gamma(\tau_2,\theta_4{=}40\text{ ns}) = 0.45$. (C) Free Ca^{2+} at 20 μM (pCa = 4.7) and sonicated SUVs. Amplitude of the (τ,θ) peak corresponding to $\tau_1 = 0.52$ ns: $\Gamma(\tau_1,\theta_1{=}0.10\text{ ns}) = 0.25$; amplitudes of the (τ,θ) peaks corresponding to $\tau_2 = 2.39$ ns: $\Gamma(\tau_2,\theta_2{=}0.10\text{ ns}) = 0.28$; $\Gamma(\tau_2,\theta_3{=}3\text{ ns}) = 0.14$; $\Gamma(\tau_2,\theta_4{>}100\text{ ns}) = 0.33$. Conditions were as described in the legend of Figure 6.

form of the protein, the short-lived excited-state population corresponds to a freely rotating conformer. The major lifetime is coupled both to this fast motion and to a long rotational correlation time of ~40 ns, which describes the Brownian rotation of the protein. It exhibits therefore a partially hindered rotational motion, with a semiangle of the wobbling-in-cone motion ω_{max} of 26°, on the same order of magnitude as in the apo form. This long rotational correlation time of ~40 ns is, however, larger than expected for the Brownian motion of the p36 protein (~15 ns). It is possible that a self-association process occurs in the presence of Ca^{2+} like we also observed for Anx5 (*55*).

Like in p36, the one-dimensional model applied to the polarized fluorescence decay of W212 in p90 shows only one rotational correlation time distribution centered at ~45 ns (Table 2). This value is slightly larger than expected from the size of the complex. The wobbling angle of rotation displays a value similar to that in p36. The two-dimensional analysis shows that the shortest lifetime is specifically coupled with a sub-nanosecond rotational motion (~500 ps) (Figure 7A,B). The major lifetime population is mainly associated with a long rotational correlation time, which displays however a value (10−12 ns) significantly smaller than that expected from the Brownian motion of a protein of the size of the heterotetramer (94 kDa) (~38 ns for a sphere with a hydration ratio of 40% w/w). We might assume that this motion could be due to a nanosecond flexibility. This lifetime is also associated with a fast rotation. The value of the semiangle of the wobbling-in-cone motion for this fast rotation is 23°, lower than the value obtained for p36. Ca^{2+} binding suppresses almost completely the peak corresponding to the nanosecond flexibility observed in the absence of calcium. A peak corresponding to the expected Brownian rotational correlation time of the complex (~40 ns) is then observed. The wobbling-in-cone angle of the sub-nanosecond rotation in the p90−Ca^{2+} complex calculated from the $\Gamma(\tau,\theta)$ coefficients, listed in the legend of Figure 7, is increased (33°) with respect to p36 and to p90 in the absence of Ca^{2+}. As remarked previously, both the one- and two-dimensional analyses provide similar low χ^2 values.

Effect of Binding of p36 and p90 to Negatively Charged Membranes on the Local Conformation and Dynamics around W212: Excited-State Lifetime Distributions. The excited-state lifetime distribution of W212 is modified upon Ca^{2+}-dependent binding of p36 and p90 to phospholipid membranes (Figures 2C and 4C and Table 1). This change is the same as that observed in the presence of Ca^{2+} alone. The Ca^{2+} concentration for the half-effect on the amplitudes of the major lifetime populations is, however, lower in the presence of phospholipid membranes than in their absence (see Figure 3, where only the data for the 2.6 ns component are presented). The half-titration point for p36 is at 0.13 mM, a concentration ~5 times lower than in the absence of phospholipid membranes (~0.7 mM). This concentration is very close to that at which membrane aggregation takes place (~0.1 mM), whereas binding of p36 to phospholipid membranes occurs in the micromolar range (~3 μM) (Figure 3A).

The Ca^{2+}-induced local conformational change in domain III in the presence of membranes exhibits a much stronger calcium sensibility for p90 than for p36 (Figure 3B). The half-titration point for p90 occurs at sub-micromolar calcium concentration (~0.7 μM), lower by more than 2 orders of magnitude than that for p36 (Figure 3B). The membrane binding and aggregation efficiency are in the same sub-micromolar Ca^{2+} concentration range (Figure 3B; J. Ayala-Sanmartin, manuscript submitted for publication). Such a higher sensitivity to calcium of p90 (which occurs in the intracellular Ca^{2+} concentration range) could produce a threshold response of the complex to calcium burst in the cells.

Effect of Membrane Binding of p36 and p90 on the Local Mobility of W212: Fluorescence Anisotropy Decays. The pattern of the impulse fluorescence anisotropy decay of W212 in the complex of either p36 or p90 with negatively charged phospholipid membranes is similar to that presented in Figure 5B. The same remarks about the model dependence hold therefore for this set of data as for the previous ones. The analysis of the polarized data by the one-dimensional model provides optimal χ^2 values of ~1, like in the absence of membranes. Only one significant rotational correlation time is observed. The initial anisotropy value is much lower than that expected for an immobilized tryptophan (*53*). No infinite anisotropy is detected by this analysis, which is quite surprising for a protein known to interact strongly with the membranes.

The two-dimensional analysis of the polarized fluorescence decays shows that in both p36 and p90, the short lifetimes are coupled only to a fast sub-nanosecond rotational motion (Figures 6C and 7C). This value is lower than that observed in the absence of membranes, but a contribution of scattered light by the aggregated vesicles cannot be excluded. The major lifetime of 2.4−2.6 ns is coupled to this fast motion and also to an intermediate nanosecond one and to a very slow motion with an infinite time constant (as compared to the excited-state lifetime). The presence of an infinite anisotropy component is classically expected for a protein firmly bound to membrane systems. This observation again favors the two-dimensional analysis with respect to the one-dimensional model. Each lifetime population likely corresponds, therefore, to conformers with different mobilities. The semiangle of the wobbling-in-cone sub-nanosecond rotational motion, calculated for the major conformer, has a value of 35° for p36 and a larger one for p90 (42°). They are both significantly larger than that observed for the Ca^{2+}-free or Ca^{2+}-bound proteins.

DISCUSSION

The binding of calcium to Anx2 is known to induce a local conformational change leading to a significant blue shift of the fluorescence emission spectrum of W212 (*26*, *28*, *30*, *31*), but affecting poorly its quantum yield (*56*). Calcium binding did not significantly alter the overall secondary structure of the protein; the decrease in the α-helix content induced by calcium was only 1−2% (*7*). In the work presented here, the time-resolved fluorescence intensity decay data clearly show that the conformational change of p36 induced by Ca^{2+} binding corresponds to a modification of the local interactions of the indole ring with specific proximate quenching moieties of the protein, which leads to changes in the major lifetime value. Former time-resolved fluorescence intensity studies have not been able to show any large change in the excited-state lifetime values of the

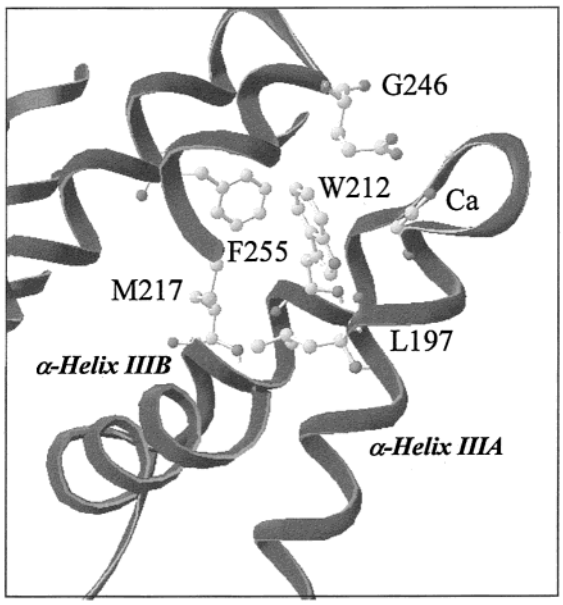

FIGURE 8: Environment of W212 in the Anx2−Ca^{2+} three-dimensional structure (*25*). This representation was rendered by the Swiss-PdbViewer (*67*).

W212 emission as a function of calcium. This was probably due to a lower time resolution of the instrumentation and a lower accuracy of the analysis at the time of the measurements (*30*, *56*). Moreover, no fluorescence anisotropy decay measurements were reported to describe the effects of calcium and membrane binding to the protein on the W212 internal dynamics. Such measurements were performed in this paper and analyzed using two models: associative and nonassociative. It turns out that classical statistical criteria cannot be used to distinguish the two. Using genuine statistics, we cannot therefore rule out the simpler, nonassociative models where each lifetime is correlated with every rotational motion. The impulse fluorescence anisotropy decays are nevertheless not described by a simple sum of exponentials; negative pre-exponential factors are needed. The two-dimensional analysis allows moreover recovery of a physically meaning value of the Brownian rotational correlation times of the proteins in the absence of membranes and also an infinite anisotropy in their presence. This was not the case with the simpler one-dimensional model. These observations suggest that the two-dimensional analysis is likely less biased by the fluorescence emission heterogeneity than the two-dimensional one.

The three-dimensional structure of the protein, which has been determined in the presence of bound Ca^{2+} (*25*), allows interpretation of to some extent the spectroscopic characteristics of W212. This residue belongs to the α-helix IIIB and is encased between α-helices IIIA and IIIB with no polar amino acid side chains in its neighborhood. The indole ring undergoes a single polar contact involving its N_ϵ atom, which likely forms a H-bond bridge with the CO group of the L197 peptide bond (3.25 Å) in α-helix IIIA (Figure 8). No other peptide bonds or polar quenching groups are present in the vicinity of W212 in the p36−Ca^{2+} complex (within a sphere of 4 Å drawn from each atom of the indole ring). This would explain the relatively "long" lifetime value of W212 in the p36−Ca^{2+} complex, since peptide bonds are efficient quenchers only when the indole ring interacts with two of them (*57*). The extremely blue fluorescence emission of W212 at ~312 nm in the presence of Ca^{2+} (*27*, *28*, *30*, *31*) fully agrees with the location of this aromatic residue in a hydrophobic cavity in the three-dimensional structure. Moreover, the orientation of the indole long axis (and approximately of its dipole moment) (*58*) is roughly perpendicular to that of α-helix IIIB (Figure 8). Such an orientation will also inhibit the possible dipolar interaction of the indole excited state with this macrodipole.

With the protein structure in the absence of Ca^{2+} still unknown, the Ca^{2+}-induced structural changes of the W212 environment accounting for the fluorescence changes can only be supposed. No significant change in the accessibility of the indole ring to the solvent has been evidenced either by acrylamide or by iodide quenching experiments (*31*, *56*). A change in the relative orientation of the indole ring with respect to the α-helix IIIB may lead to modification of dipolar interactions. The possibility that the crystal conformation of the protein is not replicated in detail in solution and that other dipoles are present in the structure around W212 should, however, remain open.

One important result reported in this work concerns the absence of local structural disturbance of the W212 region upon formation of the heterotetramer complex with the p11 dimer. The interaction of the p36 N-terminal distal part with p11 to form the heterotetrameric complex does not appear to affect the conformation of the convex face, situated at the opposite side of the protein. Nevertheless, the p90 heterotetramer exhibits flexibility in the nanosecond range detected by the two-dimensional analysis, which could not be observed in the p36 monomer. This nanosecond flexibility of p90 is likely large in amplitude since the Brownian rotational correlation time of the protein cannot be detected. It could correspond to hinge bending motions of domains in the heterotetramer. Ca^{2+} binding suppresses this nanosecond flexibility and rigidifies the protein. The interaction of the N-terminal segment of p36 with p11 could therefore affect the relative motions of domains in p90 by suppressing existing interactions of this sequence with the concave face of the core. Such interactions between an N-terminal sequence and the core have recently been shown to exist in the crystal structure of Anx3 (*59*). In this case, this interaction occurs via the W5 residue, located in the hinge region of the hydrophilic channel formed between domains II and IV. Mutation of this residue has resulted in a change in the Ca^{2+}-dependent interaction of the mutated protein with negatively charged phospholipid membranes (*60*). Therefore, although the structures of both N-terminal domains are obviously different, because of their differences in length and amino acid composition, a role of the N-terminal domain of Anx2 in the modulation of the dynamics of the core is not excluded and may help to explain the different behaviors of p36 and p90.

The most striking result of this work concerns in fact the large increase in the sensitivity to Ca^{2+} of the domain III conformational change for p90 with respect to that of p36 in the presence of membranes. A shift by more than 2 orders of magnitude of the midpoint effect of calcium concentration needed for the conformational transition is observed for the p90 tetramer with respect to the p36 monomer. To explain these observations, a further conformational change of the Ca^{2+} binding sites occurring on the membrane surface has been proposed (*31*). Our results indicate, however, that the

conformational change provoked by the Ca^{2+}-dependent binding of the protein to the membranes is the same as the change induced by Ca^{2+} alone. A significant increase in the local dynamics around the W212 residue is, however, observed in both p36 and more importantly for p90. A similar observation was reported for Anx5 bound to negatively charged phospholipid membranes (*45*). This phenomenon might be related to the global conformational changes observed by infrared measurements on this latter protein, characterized by the appearance of nonhelical structures and by the decrease in the structural order of the protein at the membrane surface (*61*, *62*).

Besides these differences in protein dynamics, the stronger cooperativity of the conformational change of p90 with respect to p36 in the presence of membranes may involve other factors. The major difference between these two Anx2 forms obviously concerns their association states and therefore the number of their Ca^{2+}-binding sites. The more efficient membrane aggregation process of p90 can be related to the existence of two surfaces of interaction with the membranes according to its assumed heterotetrameric structure (*63*). A symmetric unit containing four Ca^{2+} sites on each side will allow the apposition of two membranes, resulting in a further increase in the local Ca^{2+} concentration and a stronger reduction of dimensionality than with the monomer. It has been shown that p90 binds ~1.5 times more Ca^{2+} ions than p36 does (*29*). This increase in the number of potential Ca^{2+} contact sites with the membrane surface would decrease the apparent dissociation constant of p90 with respect to p36. This would explain the difference in Ca^{2+} concentration for membrane binding of p36 and p90 (~3 and 0.3 μM, respectively). In contrast, as shown in this work, the membrane aggregation processes occur at 0.1 mM and 0.2 μM Ca^{2+} for p36 and p90, respectively, in agreement with previous reports (*16*, *29*, *64*). Thus, the higher sensitivity to Ca^{2+} of the p90 conformational change is not associated with a difference in the Ca^{2+}-mediated binding of the proteins to the membranes, but parallels the efficiency of their Ca^{2+}-dependent membrane aggregation.

Our results suggest a tendency of p36 to dimerize in solution at high Ca^{2+} concentrations likely as a dimer, in agreement with the former results (*65*). Moreover, a calcium-dependent Anx2−Anx2 interaction also occurs at the membrane surface (*63*). The observed Ca^{2+}-induced local conformational change is not correlated with membrane binding but with membrane aggregation. In the p90 form, in which two p36 molecules are preassociated, the Ca^{2+} requirement is low, whereas for the monomer, the conformational change leading to the aggregation efficient form of the protein needs higher calcium concentrations. This suggests that the difference in sensitivity of the Ca^{2+}-dependent aggregation of membranes mediated by p36 and by p90 could be due to the difference in the mechanism of their autoassociation. We have recently shown that modification of the N-terminal sequence by site-directed mutagenesis decreases the Ca^{2+} sensitivity of the p36-mediated membrane aggregation (J. Ayala-Sanmartin, unpublished results). The self-association of p36 at the membrane surface, allowing membrane aggregation, could be due to a folding of the N-terminal segment in such a way that it does not interfere anymore with the protein core.

ACKNOWLEDGMENT

The technical staff of LURE is acknowledged for running the synchrotron ring during the beam sessions. J.A.-S. acknowledges J. P. Henry and P. Gouache for helpful discussions and support. We thank Dr. Andreas Hofmann (MPI, Martinsried, Germany) for Anx2 coordinates.

REFERENCES

1. Raynal, P., and Pollard, H. B. (1994) *Biochim. Biophys. Acta 1197*, 63−93.
2. Gerke, V., and Moss, S. E. (1997) *Biochim. Biophys. Acta 1357*, 129−154.
3. Swairjo, M. A., and Seaton, B. A. (1994) *Annu. Rev. Biophys. Biomol. Struct. 23*, 193−213.
4. Glenney, J. (1985) *FEBS Lett. 192*, 79−82.
5. Radke, V.; Gilmore, T., and Martin, G. S. (1980) *Cell 21*, 821−828.
6. Erikson, K., and Erikson, R. L. (1980) *Cell 21*, 829−836.
7. Gerke, V., and Weber, K. (1985) *J. Biol. Chem. 260*, 1688−1695.
8. Gerke, V., and Weber, K. (1984) *EMBO J. 3*, 227−233.
9. Ali, S. M., Geisow, M. J., and Burgoyne, R. D. (1989) *Nature 340*, 313−315.
10. Sarafian, T., Pradel, L. A., Henry, J. P., Aunis, D., and Bader, M. F. (1991) *J. Cell Biol. 114*, 1135−1147.
11. Emans, N., Gorvel, J. P., Walter, C., Gerke, V., Kellner, R., Griffiths, G., and Gruenberg, J. (1993) *J. Cell Biol. 120*, 1357−1369.
12. Harder, T., and Gerke, V. (1993) *J. Cell Biol. 123*, 1119−11132.
13. Mayorga, L. S., Beron, W., Sarrouf, M. N., Colombo, M. I., Creutz, C., and Stahl, P. D. (1994) *J. Biol. Chem. 269*, 30927−30934.
14. König, J., Prenen, J., Nilius, B., and Gerke, V. (1998) *J. Biol. Chem. 273*, 19679−19684.
15. Glenney, J. (1986) *J. Biol. Chem. 261*, 7247−7252.
16. Powell, M. A., and Glenney, J. R. (1987) *Biochem. J. 247*, 321−328.
17. Glenney, J. R. J., Boudreau, M., Galyean, R., Hunter, T., and Tack, B. (1986) *J. Biol. Chem. 261*, 10485−10488.
18. Johnsson, N., Marriott, G., and Weber, K. (1988) *EMBO J. 7*, 2435−2442.
19. Becker, T., Weber, K., and Johnsson, N. (1990) *EMBO J. 9*, 4207−4213.
20. Réty, S., Sopkova, J., Renouard, M., Osterloh, D., Gerke, V., Tabaries, S., Russo-Marie, F., and Lewit-Bentley, A. (1999) *Nat. Struct. Biol. 6*, 89−95.
21. Jost, M., and Gerke, V. (1996) *Biochim. Biophys. Acta 1313*, 283−289.
22. Glenney, J. R., and Tack, B. F. (1985) *Proc. Natl. Acad. Sci. U.S.A. 82*, 7884−7888.
23. Johnsson, N., Van Phuc, N., Söling, H.-D., and Weber, K. (1986) *EMBO J. 5*, 3455−3460.
24. Gould, K. L., Woodgett, J. R., Isacke, C. M., and Hunter, T. (1986) *Mol. Cell. Biol. 6*, 2738−2744.
25. Burger, A., Berendes, R., Liemann, S., Benz, J., Hofmann, A., Göttig, P., Huber, R., Gerke, V., Thiel, C., Römisch, J., and Weber, K. (1996) *J. Mol. Biol. 257*, 839−847.
26. Jost, M., Thiel, C., Weber, K., and Gerke, V. (1992) *Eur. J. Biochem. 207*, 923−930.
27. Jost, M., Weber, K., and Gerke, V. (1994) *Biochem. J. 298*, 553−559.
28. Thiel, C., Weber, K., and Gerke, V. (1991) *J. Biol. Chem. 266*, 14732−14739.
29. Evans, T. C. J., and Nelsestuen, G. L. (1994) *Biochemistry 33*, 13231−13238.
30. Marriott, G., Kirk, W. R., Johnsson, N., and Weber, K. (1990) *Biochemistry 29*, 7004−7011.
31. Pigault, C., Follénius-Wund, A., Lux, B., and Gérard, D. (1990) *Biochim. Biophys. Acta 1037*, 106−114.
32. Follenius-Wund, A., Pigault, C., and Gerard, D. (1993) *Biochem. Mol. Biol. Int. 29*, 653−660.

33. Bazzi, M. D., and Nelsestuen, G. L. (1991) *Biochemistry 30*, 971−979.
34. Bandorowicz, J., Pikula, S., and Sobota, A. (1992) *Biochim. Biophys. Acta 1105*, 201−206.
35. Giga-Hama, Y., Tohda, H., Okada, H., Owada, M. K., Okayama, H., and Kumagai, H. (1994) *Bio/Technology 12*, 400−404.
36. Ayala-Sanmartin, J., Henry, J. P., and Pradel, L. A. (2000) *Biochim. Biophys. Acta* (in press).
37. Föhr, K. J., Warchol, W., and Gratzl, M. (1993) *Methods Enzymol. 221*, 149−157.
38. Vincent, M., Gallay, J., and Demchenko, A. D. (1995) *J. Phys. Chem. 99*, 14931−14941.
39. Livesey, A. K., and Brochon, J.-C. (1987) *Biophys. J. 52*, 693−706.
40. Vincent, M., Brochon, J. C., Merola, F., Jordi, W., and Gallay, J. (1988) *Biochemistry 27*, 8752−8761.
41. Brochon, J.-C. (1994) *Methods Enzymol. 240*, 262−311.
42. Vincent, M., and Gallay, J. (1991) *Eur. Biophys. J. 20*, 183−191.
43. Rouvière, N., Vincent, M., Craescu, C. T., and Gallay, J. (1997) *Biochemistry 36*, 7339−7352.
44. Sopkova, J., Vincent, M., Takahashi, M., Lewit-Bentley, A., and Gallay, J. (1998) *Biochemistry 37*, 11962−11970.
45. Sopkova, J., Vincent, M., Takahashi, M., Lewit-Bentley, A., and Gallay, J. (1999) *Biochemistry 38*, 5447−5458.
46. Brand, L., Knutson, J. R., Davenport, L., Beechem, J. M., Dale, R. E., Walbridge, D. G., and Kowalczyk, A. A. (1985) in *Spectroscopy and the Dynamics of Molecular Biological Systems* (Bayley, P., and Dale, R. E., Eds.) pp 259−305, Academic Press, London.
47. Lakowicz, J. R. (1999) in *Principles of Fluorescence Spectroscopy* (Lakowicz, J. R., Ed.) pp 362−365, Kluwer Academics/Plenum Publishers, New York.
48. Ruggiero, A., and Hudson, B. (1989) *Biophys. J. 55*, 1125−1135.
49. Ludescher, R. D., Peting, L., Hudson, S., and Hudson, B. (1987) *Biophys. Chem. 28*, 59−75.
50. Guest, C. R., Hochstrasser, R. A., Dupuy, C. G., Allen, D. J., Benkovic, S. J., and Millar, D. P. (1991) *Biochemistry 30*, 8759−8770.
51. Bialik, C. N., Wolf, B., Rachojski, E. L., Ross, J. B. A., and Laws, W. R. (1998) *Biophys. J. 75*, 2564−2573.
52. Vincent, M., Rouvière, N., and Gallay, J. (2000) *Cell. Mol. Biol. 46*, 1113−1131.
53. Valeur, B., and Weber, G. (1977) *Photochem. Photobiol. 25*, 441−444.
54. Kinosita, K. J., Kawato, S., and Ikegami, A. (1977) *Biophys. J. 20*, 289−305.
55. Sopkova, J., Gallay, J., Vincent, M., Pancoska, P., and Lewit-Bentley, A. (1994) *Biochemistry 33*, 4490−4499.
56. Pigault, C., Follenius-Wund, A., and Gérard, D. (1990) *Biochem. Soc. Trans. 18*, 1229−1230.
57. Chen, Y., and Barkley, M. D. (1998) *Biochemistry 37*, 9976−9982.
58. Callis, P. (1997) *Methods Enzymol. 278*, 113−150.
59. Favier-Perron, B., Lewit-Bentley, A., and Russo-Marie, F. (1996) *Biochemistry 35*, 1740−1744.
60. Hofmann, A., Raguénès-Nicol, C., Favier-Perron, B., Mesonero, J., Huber, R., Russo-Marie, F., and Lewit-Bentley, A. (2000) *Biochemistry 39*, 7712−7721.
61. Silvestro, L., and Axelsen, P. H. (1999) *Biochemistry 38*, 113−121.
62. Wu, F., Flach, C. R., Seaton, B. A., Mealy, T. R., and Mendelsohn, R. (1999) *Biochemistry 38*, 792−799.
63. Lambert, O., Gerke, V., Bader, M. F., Porte, F., and Brisson, A. (1997) *J. Mol. Biol. 272*, 42−55.
64. Drust, D. S., and Creutz, C. E. (1988) *Nature 331*, 88−91.
65. Liu, L. (1999) *Cell. Signalling 11*, 317−324.
66. Wahl, P. (1979) *Biophys. Chem. 10*, 91−104.
67. Guex, N., Diemand, A., and Peitsch, M. C. (1999) *Trends Biochem. Sci. 24*, 364−367.

BI000501X